Hindawi
Journal of Chemistry
Volume 2021, Article ID 2672674, 18 pages
https://doi.org/10.1155/2021/2672674

Research Article

Preparation of Ti/SnO_2-Sb/Rare Earth Electrodes Containing Different Contents of Ni Intermediate Layer for Efficient Electrochemical Decolorization of Rhodamine B

Thet Phyo Wai, Yilin Yin, Xiao Zhang, and Zenghe Li

Beijing Key Laboratory of Environmentally Harmful Chemical Analysis, College of Chemistry, Beijing University of Chemical Technology, Beijing 100029, China

Correspondence should be addressed to Zenghe Li; lizh@mail.buct.edu.cn

Received 12 April 2021; Revised 6 May 2021; Accepted 20 May 2021; Published 31 May 2021

Academic Editor: Fadi Alakhras

Water contamination by dyes discharged from many industries is an environmental issue of great matter. Electrochemical oxidation is an advanced approach for wastewater treatment. In this study, the composite electrodes of Ti/SnO_2-Sb-Ni/rare earth have been modified using rare earth elements (Re) Gd, Ce, Eu, and Er and various molar ratios of tin and nickel intermediate layer, and their electrochemical oxidation effects were scrutinized. To analyze the decolorization performance of the electrodes, Rhodamine B (RhB) dye was utilized as a target pollutant. Accelerated life testing indicated that the longer service life could be observed in Ni (3.5%)/Re and Ni (5%)/ Re electrodes compared with other modified Ni (0%, 1%, and 2%)/Re electrodes. Compared with the color removal efficiencies of the Ni (2%)/Re electrodes, the decolorization rate of 90% after treatment for 60 min and the low energy consumption of 3.621 kW h·m^{-3} can be achieved at the Ni (2%)/Gd electrode under the experimental condition of 100 mg·L^{-1} RhB. The best decolorization rate was observed at the Ni (2%)/Re electrodes among other Ni and no adding Ni-doped Re electrodes. The characterization of the electrodes was described, consisting of surface morphology, oxygen evolution potential, and a crystallographic and elemental combination of the coatings.

1. Introduction

Pollution of water sources by wastewater from synthetic dye and textile industries is the main cause of water pollution since their released wastewater could contain continual organic dyes and harmful by-products. Leftover coloring matters are distinguished by intense color, high organic content, and steady chemical composition due to the existence of azo functional groups. Therefore, they have influenced serious hazards for the environment and human beings [1, 2]. These environmental impact dyes are degraded by various treatment techniques such as biological degradation system [3], adsorption [4], coagulation-flocculation [5], Fenton technique [6], membrane separation [7], photocatalysis [8], son-catalysis, and ozonation [9, 10].

The pollutants oxidized by the electrochemical processes have also been accepted as an impressive method for decolorizing wastewaters and to degrade dyes because of their advantages: safety and ease to operate, wide scope of treatment conditions, and ecological similarity [11–16]. The hydroxyl radicals ($^{\cdot}OH$) are generated when the electrochemical oxidation transforms several pollutants into carbon dioxide, water, and some inorganic anions [17–19]. Four requirements have been needed to possess an excellent modified electrode: remarkable electrocatalytic activity, high oxygen evolution potential, excellent service life, and good conductivity [20]. Titanium-based SnO_2-Sb is considered a suitable electrode material due to its higher OEP and superior electrochemical performance. However, the poor adhesion coating layer, easy detachment, short stability, and not high degradation achievement of the SnO2-Sb electrodes obstruct their widespread applications [21–24]. The insertion intermediate layer between an active layer and the Ti base, Ti/TiH_x/Sb-Sn [25], Ti/Cu-NRs/Sb-Sn [26], Ti/TiO_xH_y/

Sb–Sn [27] Ti/IrO_2/Sb-Sn [28], Ti/Pt/Sb-Sn [29], Ti/TiO_2-NT/Sn–Sb [30], significantly improves the performance of SnO_2–Sb electrodes. In addition, Mn is also applied as interlayers of Ti-based SnO_2 electrode because of not only cost-effective preparation but also uncomplicated preparation processes. Introducing the rare earth Gd [31], Eu, Dy [32, 33], Er [34] into the outer layer of the electrodes as dopants can also greatly affect the degradation efficiency.

In the present work, the SnO_2-Sb active layer is doped with rare earth elements (Gd, Ce, Er, and Eu), and Ni intermediate layers and no intermediate layer were prepared by brush-coating thermal pyrolysis procedure. The purpose of this work is to focus on the effects of the different intermediate layer contents on electrode electrocatalytic performance and compare them using a different initial dye concentration of RhB and stability to choose the most excellent modified electrode materials. X-ray diffraction (XRD), scanning electron microscopy (SEM), energy dispersive spectroscopy (EDS), and linear sweep voltammetry (LSV) were performed to characterize the modified electrodes.

2. Experimental

2.1. Preparation of Electrodes. Titanium substrates (20 mm × 50 mm × 0.5 mm, high purity, Bao-Ti Co. Ltd, China) were refined with abrasive papers and then ultrasonically degreased with 1 : 1 volume by volume mixture solution of 1.0 mol·L^{-1} NaOH and acetone in an ultrasonic bath for 30 min, followed by boiling in a 10% (wt.%) oxalic acid at 98°C for 120 min. The intermediate coating solution was prepared by adding a proper quantity of hydrochloric acid including 1.0 mol·L^{-1} $SnCl_4{\cdot}5H_2O$ (Sigma Aldrich), $SbCl_3$ 0.3 mol·L^{-1} (99.5%, Merck), and x mol·L^{-1} $NiCl_2{\cdot}6H_2O$ (98%, Merck) ($x = 0.01$, 0.02, 0.035 and 0.05) into n-butanol. The prepared solution for the active layer was consisting of $SnCl_4.5H_2O$ and $SbCl_3$ and suitable rare earth (Sn/Sb/Re of 100 : 3:2, molar ratio) which were added insolvent that was used the same as above. The coating layer solution for the intermediate layer was uniformly covered on the titanium plates by using a soft brush. After brushing the coating, the solution on the Ti sheet was evaporated at the oven at 120°C for 10 min. The procedure of brush and dry was done again three times, and then, thermal oxidation of the coating layer was formed at about 400°C for 10 min by a muffle furnace. This process was replicated 8 times. The last thermal decomposition process was operated at about 500°C for 60 min. Lastly, identical procedures were employed to overlay and thermally oxidized to develop the outer layer.

2.2. Characterization of Electrodes. The microstructure of the electrodes was characterized by a Bruker D8 ADVANCE X-ray diffractometer (Germany) with Cu-Kα radiation with an operating voltage of 40 kV and a current of 40 mA. The micromorphology and the microanalysis of the content of the element were observed using S-4700 field emission SEM (Hitachi Industrial Equipment Systems Co., Ltd, Japan). The oxygen evolution potential measurements of electrodes were investigated in a conventional three-electrode cell system at the electrochemical workstation (Chenhua Instrument Shanghai Co. Ltd. China). The OEP of the electrodes was tested at 10 mV·s^{-1} in 0.1 mol·L^{-1} Na_2SO_4 solution at room temperature. The as-prepared electrode (10 × 10 mm^2) was served as a working electrode. A platinum plate and Ag/AgCl electrode were served as a counter electrode and a reference electrode, respectively. To decrease the observational duration, the accelerated service lifetime test was conducted at a stable current density of 1000 mA·cm^{-2} in a 1.0 mol·L^{-1} sulfuric acid solution at 40°C. The modified electrodes served as the anode (10 × 10 mm^2) and a Ti sheet was employed as the cathode by spacing the electrodes adjusted to roundabout 10 mm. The cell potential is simultaneously noted constant time interval for evaluating electrode inactivation when the value reached 10.0 V.

2.3. Electrochemical Decolorization of Rhodamine B. In each electrochemical decolorization experiment, 200 ml dye solution with 0.1 mol·L^{-1} Na_2SO_4 as an electrolytic solution was used in a two-electrode system using 250 ml capacity of a cylinder cell. The initial dye concentration (20, 40, and 100 mg L^{-1}) was investigated to gauge the efficiency of the electrodes because actual wastewater involves various concentrations of RhB. The modified electrodes with an effective area (20 × 20 mm^2) and Ti plate were employed as an anode and cathode which were separated at approximately 20 mm of the interelectrode distance space, and a magnetic bar was used to mix thoroughly the dye solution with a steady rotation rate during the electrocatalytic process. The applied current was fitted at a consistent current intensity of 10 mA·cm^{-2} using an SS-605 switching direct current power supply. The tested samples were eliminated from the experimental system at fixed meantime examined during the dye decolorization processes. The absorbed radiation of the tested sample was measured spectrophotometrically on the model 2200 UV-visible spectrophotometer (Ocean Optics, Dunedin, FL) at the maximal absorption wavelength (554 nm). The decolorization efficiency (η) was evaluated by the following equation:

$$\text{decolorization } (\eta) = \frac{(C_0 - C_t)}{C_0} \times 100\%, \quad (1)$$

where C_0 and C_t were before degradation and after degradation time t of the concentration of RhB, respectively.

3. Results and Discussion

3.1. Characterization of Electrodes Surface. SEM morphologies of the Ti/SnO_2-Sb-Ni/Re electrodes with different Ni contents can be observed in Figures 1–4. Many reports described that during the preparation of the annealing processes, a mud crack-like structure appeared because the Ti base expands with the increase in temperature [35, 36]. The coating morphology of the Ti/SnO_2-Sb-Ni (2%)/Gd electrode is composed of smaller cracks, and a smoother coating surface is obtained (Figure 1(c)). The crack width of the Ti/SnO_2-Sb-Ni (0%)/Gd electrode (Figure 1(a)) is

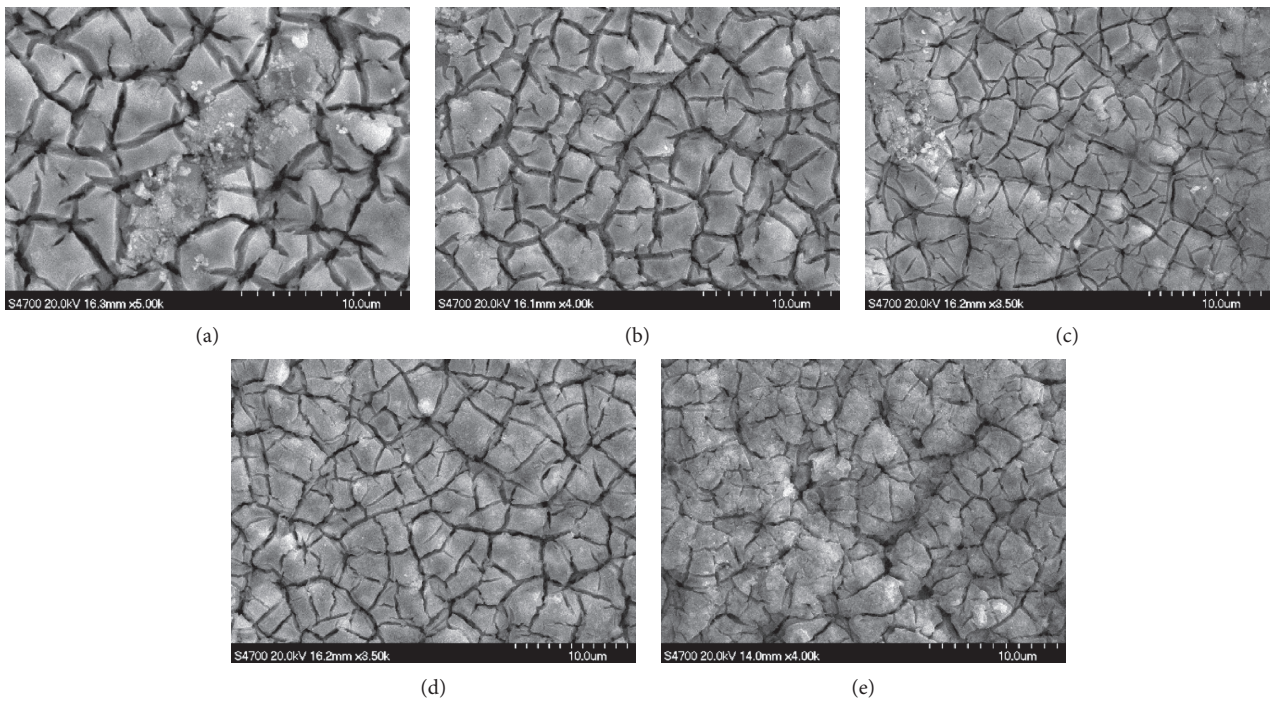

Figure 1: SEM images of Ti/SnO_2-Sb-Ni/Gd electrodes with (a) Ni (0%), (b) Ni (1%), (c) Ni (2%), (d) Ni (3.5%), and (e) Ni (5%).

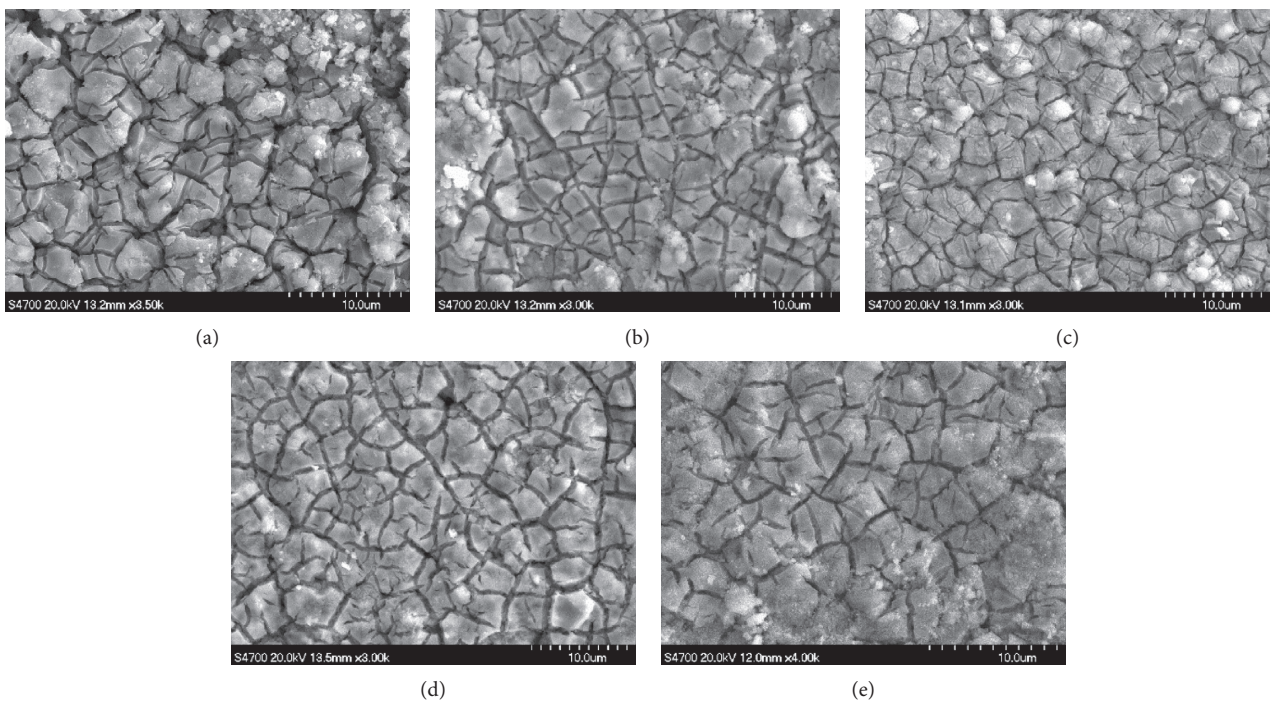

Figure 2: SEM images of Ti/SnO_2-Sb-Ni/Ce electrodes with (a) Ni (0%), (b) Ni (1%), (c) Ni (2%), (d) Ni (3.5%), and (e) Ni (5%).

correspondingly larger than the other Ti/SnO_2-Sb-Ni/Gd electrode surfaces (Figures 1(b)–1(e)). Proper crack size can boost the coating surface area. Thus, the electrochemical degradation ability of the Ti/SnO_2-Sb-Ni (2%)/Gd is the strongest among other Ti/SnO_2-Sb-Ni/Gd electrodes.

Compared with Ti/SnO_2-Sb-Ni (2%)/Ce electrode (Figure 2(c)), the solidity of Ti/SnO_2-Sb-Ni (0%)/Ce is not optimal, and some surfaces have a large number of deep cracks (Figure 2(a)). The loose cracks appear at the Ni (0%)/Ce electrode surface match with the Ni (3.5%)/Ce electrode

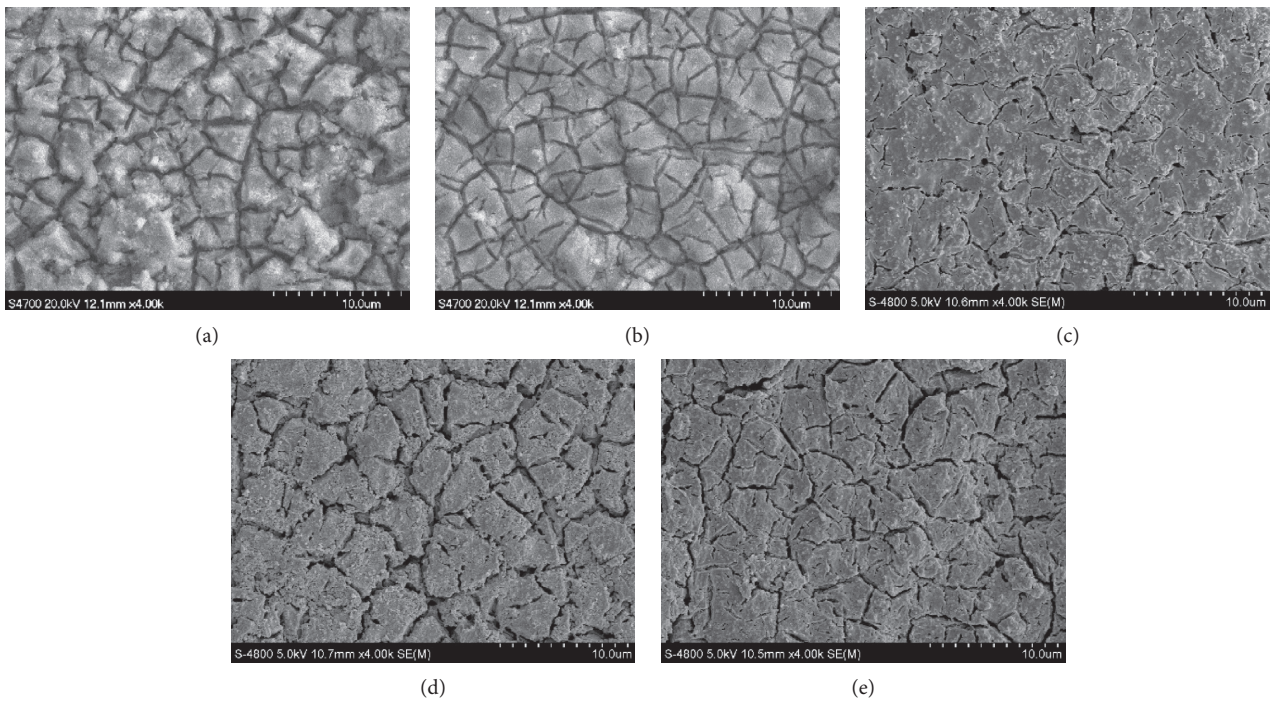

Figure 3: SEM images of Ti/SnO_2-Sb-Ni/Eu electrodes with (a) Ni (0%), (b) Ni (1%), (c) Ni (2%), (d) Ni (3.5%), and (e) Ni (5%).

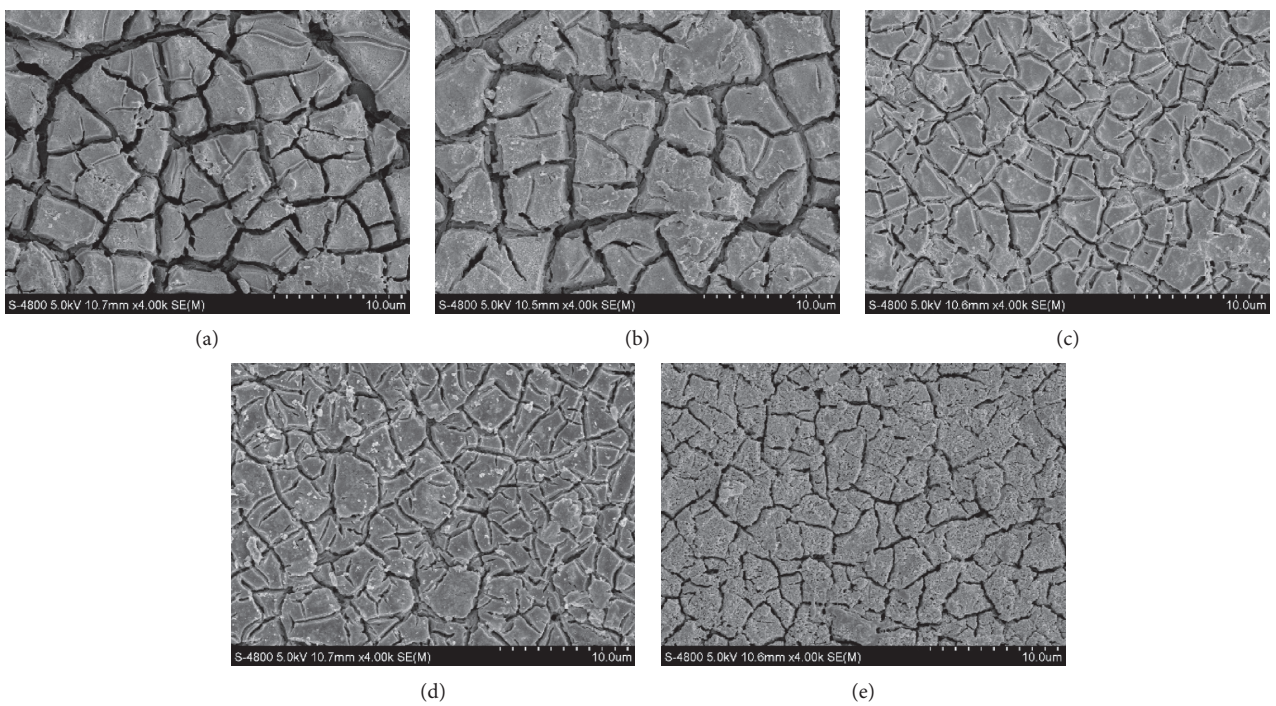

Figure 4: SEM images of Ti/SnO_2-Sb-Ni/Er electrodes with (a) Ni (0%), (b) Ni (1%), (c) Ni (2%), (d) Ni (3.5%), and (e) Ni (5%).

surface (Figure 2(d)) and Ni (5%)/Ce electrode (Figure 2(e)). Thus, the service life of the Ni (0%)/Ce electrode is not extended to reach the lifetime of these two electrodes. The smoothness and small crack size coating can also increase the electrode surface area. Hence, electrocatalytic capability of Ti/SnO_2-Sb-Ni (2%)/Ce electrode is relatively better than those of Ni (0%), Ni (1%), Ni (3.5%), and Ni (5%) of Ti/SnO_2-Sb-Ni/Ce electrodes.

Compared with other Ti/SnO_2-Sb-Ni/Eu electrodes demonstrated in Figures 3(b)–3(e), the cracks on the Ti/SnO_2-Sb-Ni (0%)/Eu electrode were not compact and smooth and have a coarse surface (Figure 3(a)). The coating

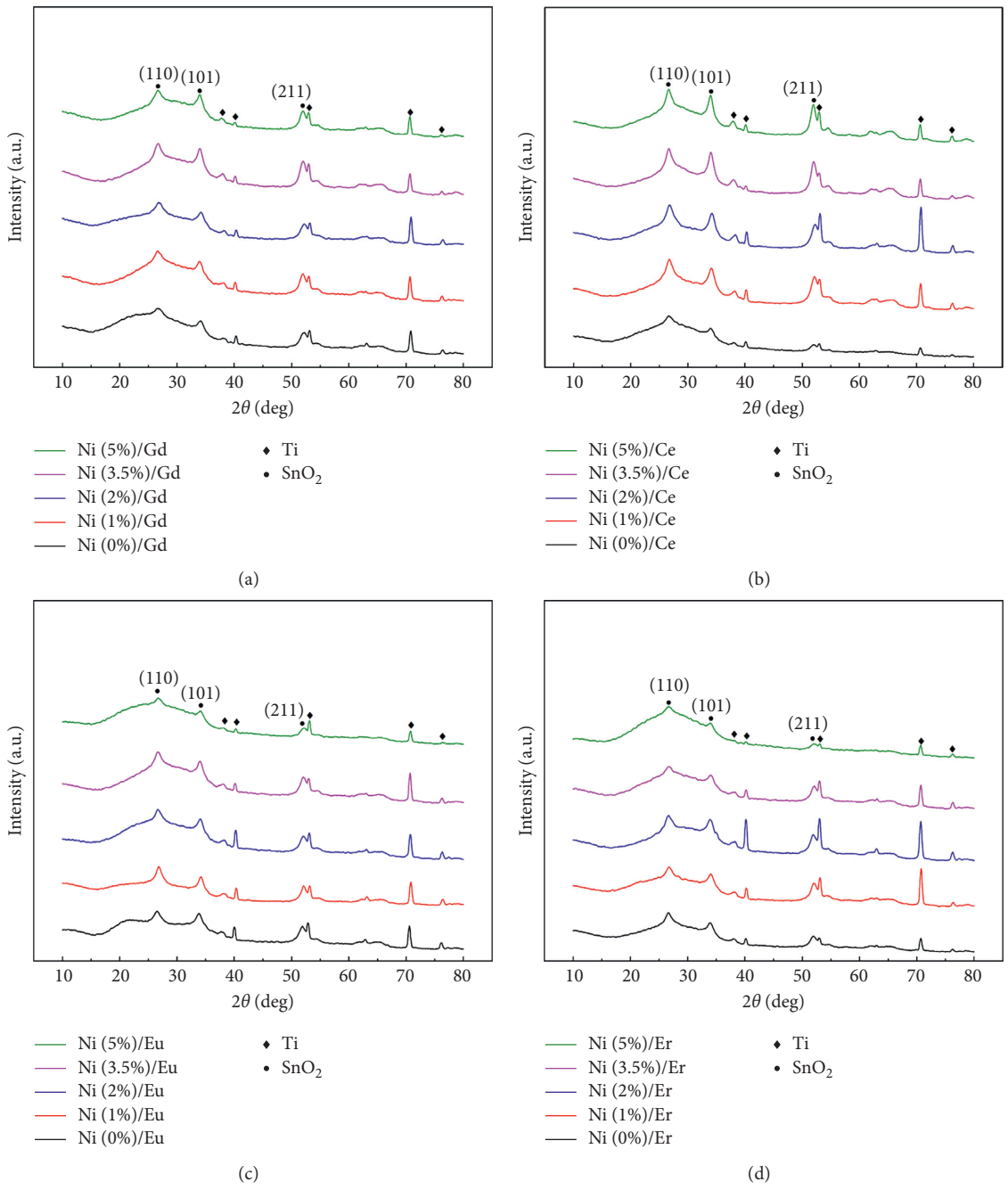

Figure 5: XRD patterns of Ti/SnO_2-Sb-Ni (0%, 1%, 2%, 3.5% and 5%)/Re electrodes. (Re = (a) Gd, (b) Ce, (c) Eu, and (d) Er).

Table 1: Coating composition of the electrodes (at. %).

Element	Percentage of element			
	Ti/SnO_2-Sb-Ni (2%)/Gd	Ti/SnO_2-Sb-Ni (2%)/Ce	Ti/SnO_2-Sb-Ni (2%)/Eu	Ti/SnO_2-Sb-Ni (2%)/Er
O	28.76	27.61	27.95	25.81
Sn	57.94	54.94	55.20	58.28
Sb	3.91	12.09	4.58	5.22
Ni	0.12	0.32	0.38	0.74
Gd	9.27	0.00	0.00	0.00
Ce	0.00	5.03	0.00	0.00
Eu	0.00	0.00	11.88	0.00
Er	0.00	0.00	0.00	9.95

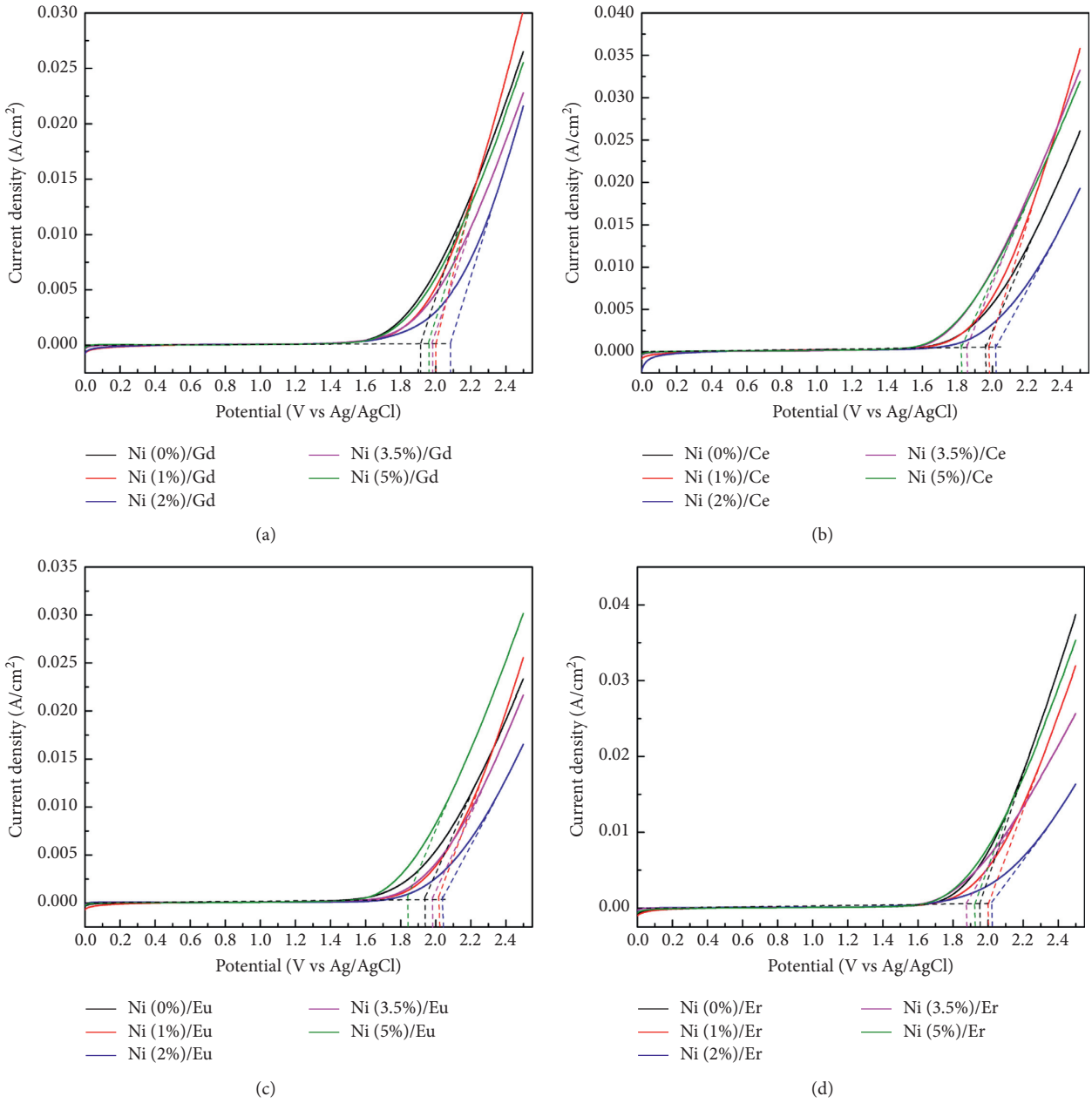

Figure 6: Linear voltammetric curves of Ti/SnO_2-Sb-Ni (0%, 1%, 2%, 3.5%, and 5%)/Re electrodes in 0.1 mol·L^{-1} Na_2SO_4 at 10 mV·s^{-1} (Re = (a) Gd, (b) Ce, (c) Eu, and (d) Er).

surface of the Ti/SnO_2-Sb-Ni (2%)/Eu electrode (Figure 4(c)) is a smoother crack area than those of the Ti/SnO_2-Sb-Ni (3.5%)/Eu electrode (Figure 3(d)) and Ti/SnO_2-Sb-Ni (5%)/Eu electrode (Figure 3(e)). Smaller cracks' size is affiliated with higher active areas. Therefore, Ti/SnO_2-Sb-Ni (2%)/Eu electrode has better performance of the electrocatalytic activity.

The coating surfaces of Ti/SnO_2-Sb-Ni (0%)/Er electrode (Figure 4(a)) and Ti/SnO_2-Sb-Ni (1%)/Er electrode (Figure 4(b)) were observed more apart and patchier and have deeper and wider cracks than other electrodes' surface (Figures 4(c)–4(e)). Loosening the compacted surface and large crack areas can easily fall off the coating from the substrate during the electrochemical degradation process as the issue of the electrolyte permeation into the electrode substrate. Uniform and composed of smaller cracks can also provide a large electroactive area. So, Ti/SnO_2-Sb-Ni (2%)/Er electrode possesses better electrocatalytic activity. The addition of Ni (2%) intermediate layer could construct to be more uniform and smoother surface than the other Ni contents and without Ni electrodes, increasing more reactive areas and improving the decolorization performance of electrodes.

According to Figures 5, XRD patterns demonstrate the titanium diffraction peak (JCPDS:44-1294) and crystalline SnO_2. The fundamental peaks were observed at 26.7°, 33.8°,

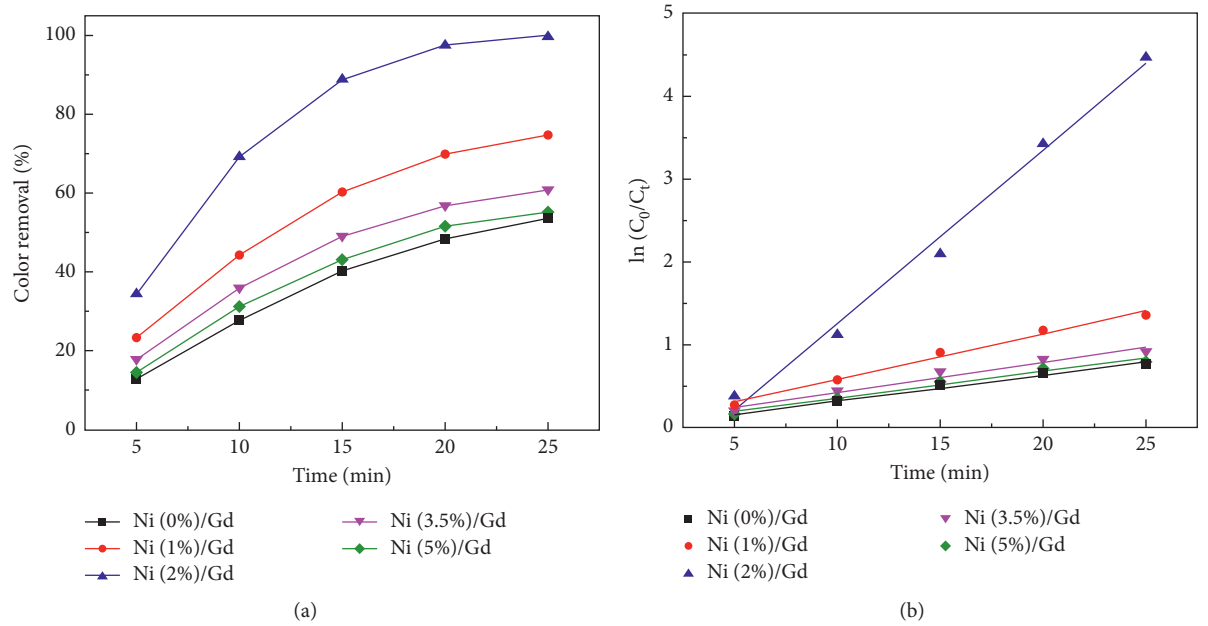

Figure 7: Electrochemical decolorization performance at Ti/SnO_2-Sb-Ni/Gd electrodes modified with various Ni contents. (a) Decolorization efficiency. (b) Kinetic analysis of the curves (RhB concentration: 20 mg·L^{-1}; current density: 10 mA·cm^{-2}; supporting electrolyte: 0.1 mol·$L^{-1}$$Na_2SO_4$; 25°C).

Table 2: Kinetic parameters of 20 mg·L^{-1} RhB in electrochemical processes by Ti/SnO_2-Sb-Ni/Gd electrodes modified with various Ni contents.

	Ni (0%)/Gd	Ni (1%)/Gd	Ni (2%)/Gd	Ni (3.5%)/Gd	Ni (5%)/Gd
Rate constants (k) (min^{-1})	0.0316	0.0554	0.2094	0.0366	0.0322
R^2	0.988	0.9863	0.9908	0.9713	0.9744

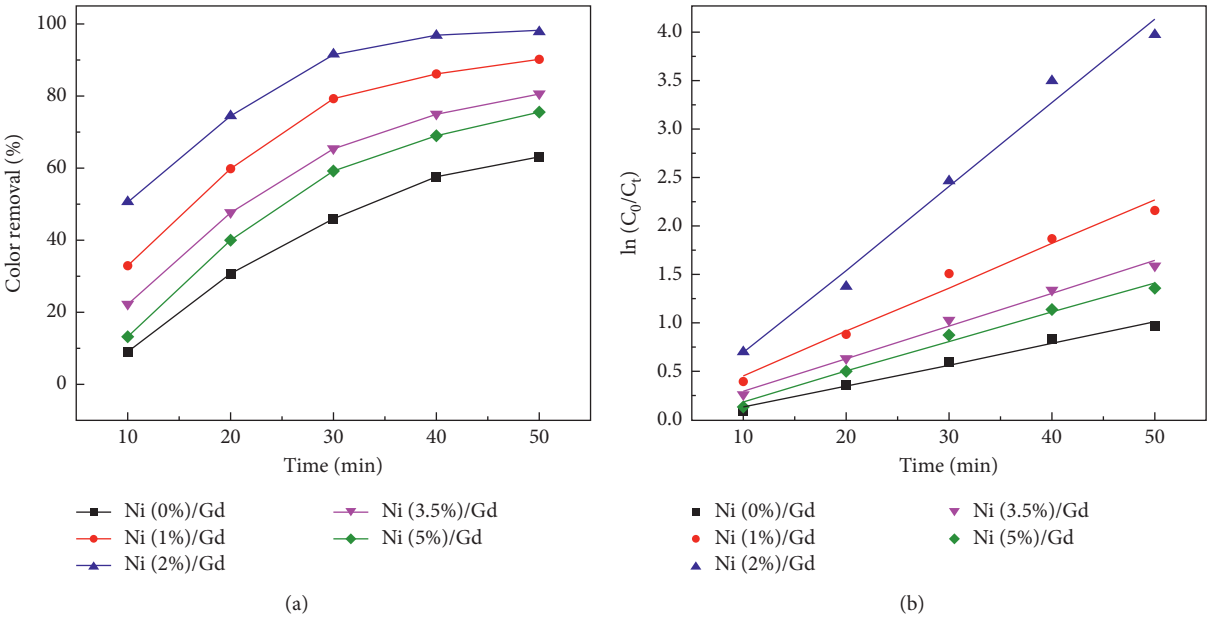

Figure 8: Electrochemical decolorization performance at Ti/SnO_2-Sb-Ni/Gd electrodes modified with various Ni contents. (a) Decolorization efficiency. (b) Kinetic analysis of the curves (RhB concentration: 40 mg L^{-1}; current density: 10 mA cm^{-2}; supporting electrolyte: 0.1 mol $L^{-1}$$Na_2SO_4$; 25°C).

Table 3: Kinetic parameters of 40 mg·L^{-1} RhB in electrochemical processes by Ti/SnO_2-Sb-Ni/Gd electrodes modified with various Ni contents.

	Ni (0%)/Gd	Ni (1%)/Gd	Ni (2%)/Gd	Ni (3.5%)/Gd	Ni (5%)/Gd
Rate constants (k) (min^{-1})	0.0221	0.045	0.0861	0.0335	0.0306
R^2	0.9875	0.9806	0.9854	0.9899	0.9877

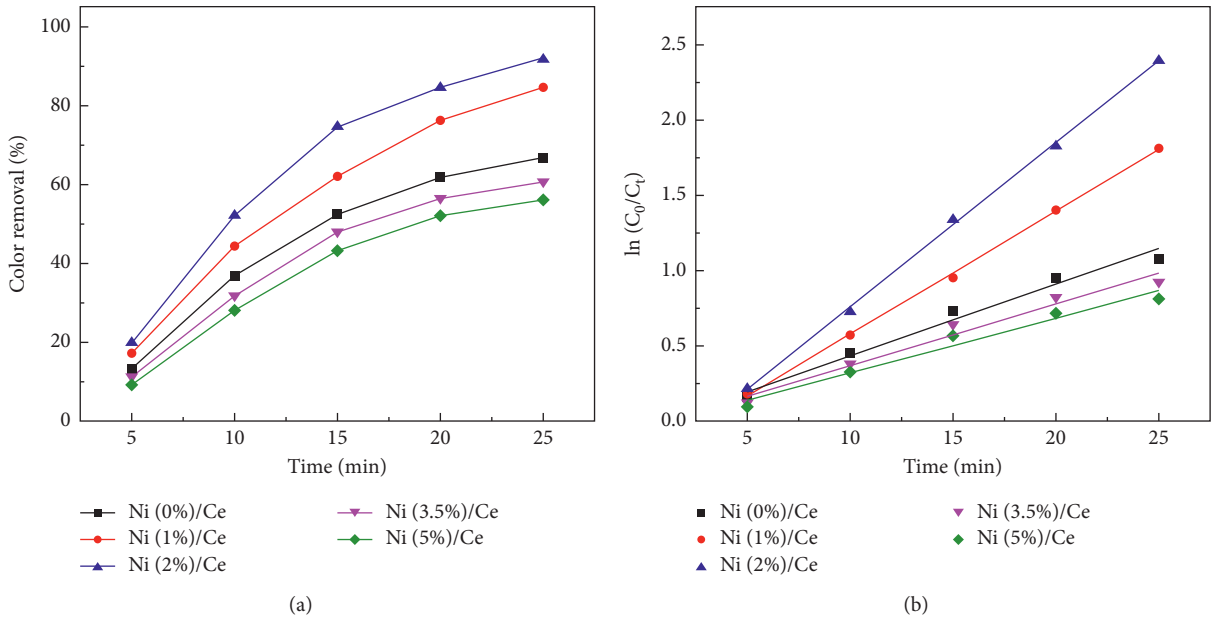

Figure 9: Electrochemical decolorization performance at Ti/SnO_2-Sb-Ni/Ce electrodes modified with various Ni contents. (a) Decolorization efficiency. (b) Kinetic analysis of the curves (RhB concentration: 20 mg·L^{-1}; current density: 10 mA·cm^{-2}; supporting electrolyte: 0.1 mol·L^{-1}Na_2SO_4; 25°C).

Table 4: Kinetic parameters of 20 mg·L^{-1} RhB in electrochemical processes by Ti/SnO_2-Sb-Ni/Ce electrodes modified with various Ni contents.

	Ni (0%)/Ce	Ni (1%)/Ce	Ni (2%)/Ce	Ni (3.5%)/Ce	Ni (5%)/Ce
Rate constants (k) (min^{-1})	0.0476	0.0817	0.109	0.0409	0.0364
R^2	0.9769	0.9989	0.999	0.9701	0.9702

and 51°, which can be agreed well with the (110), (101), and (211) crystal faces of a rutile-type structure SnO_2 cassiterite (JCPDS:41-1445). The peak at the (110) crystal face is a favored position because the intensity ratios of (101) and (211) are smaller than the strength of the (110) diffraction peak of SnO_2. The peak intensities of the SnO_2 were increased when the contents of Ni increased from 1 to 5. In any case, the decolorization performance was decreased with including Ni amount of 3.5 to 5%; as a result, these intensities increased. Thus, the inclusion of Ni 2% for all prepared electrodes is ideal for improving the decolorization activities of all as-prepared electrodes. No characteristic peaks of TiO_2 were observed, so it strongly proposed that the Ti support was not oxidized during the electrode preparation. The characteristic peaks of Sb, Ni, and Re elements were not observed in Figures 5(a)–5(d), indicating that the Sb, Ni, and Re phases were mutually entered into SnO_2 unit cells at high temperatures [37, 38]. The presence of Ni, Sn, Sb, and rare earth (Gd, Ce, Eu, and Er) could be acquired by EDS (Table 1).

3.2. Linear Sweep Voltammetry. Normally, the oxygen evolution potential is a crucial index that is utilized to gauge the electrochemical decolorization ability of an electrode. According to Figures 6(a)–6(d), the potential curve of the as-prepared electrode is partitioned into two segments. In the first segment, the current is stable as the voltage escalates, and the current mounts suddenly in the second segment as a result of raising potential. The oxygen evolution reaction distinctly appeared at the mounting site of the curve. At the second segment, a straight line that touches the curve is illustrated where the curve immediately increases, and the potential of the converging point where the straight line of

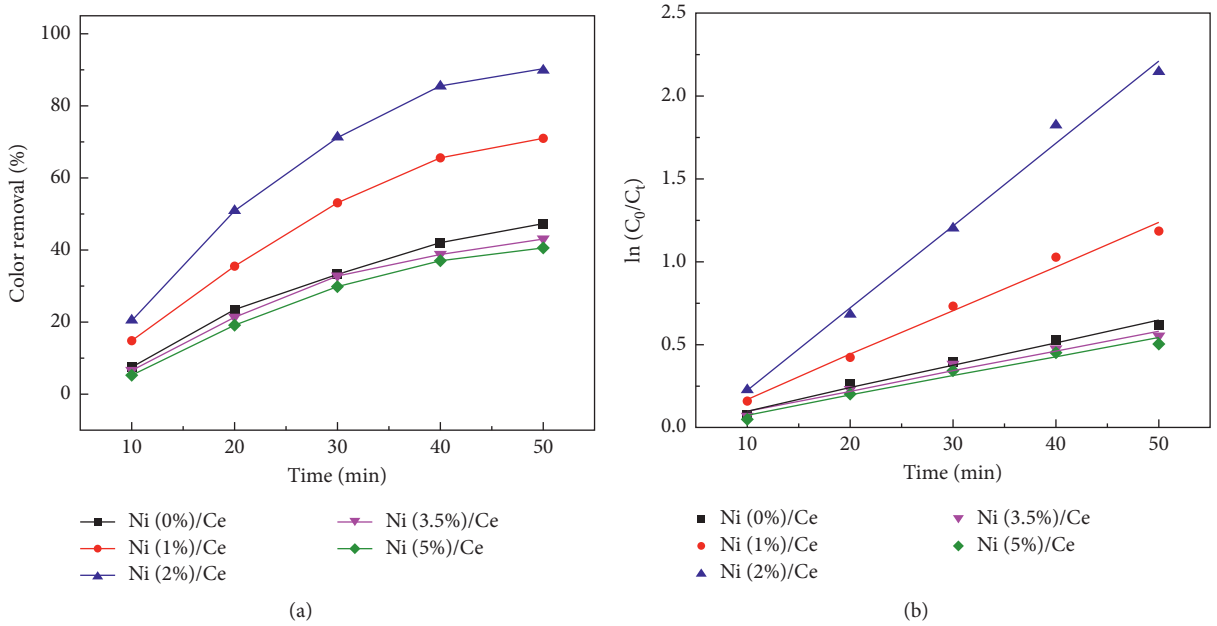

Figure 10: Electrochemical decolorization performance at Ti/SnO_2-Sb-Ni/Ce electrodes modified with various Ni contents. (a) Decolorization efficiency. (b) Kinetic analysis of the curves (RhB concentration: 40 mg·L^{-1}; current density: 10 mA·cm^{-2}; supporting electrolyte: 0.1 mol·$L^{-1}$$Na_2SO_4$; 25°C).

Table 5: Kinetic parameters of 40 mg·L^{-1} RhB in electrochemical processes by Ti/SnO_2-Sb-Ni/Ce electrodes modified with various Ni contents.

	Ni (0%)/Ce	Ni (1%)/Ce	Ni (2%)/Ce	Ni (3.5%)/Ce	Ni (5%)/Ce
Rate constants (k) (min^{-1})	0.0136	0.0265	0.0498	0.0121	0.0116
R^2	0.9863	0.99	0.9931	0.9705	0.9711

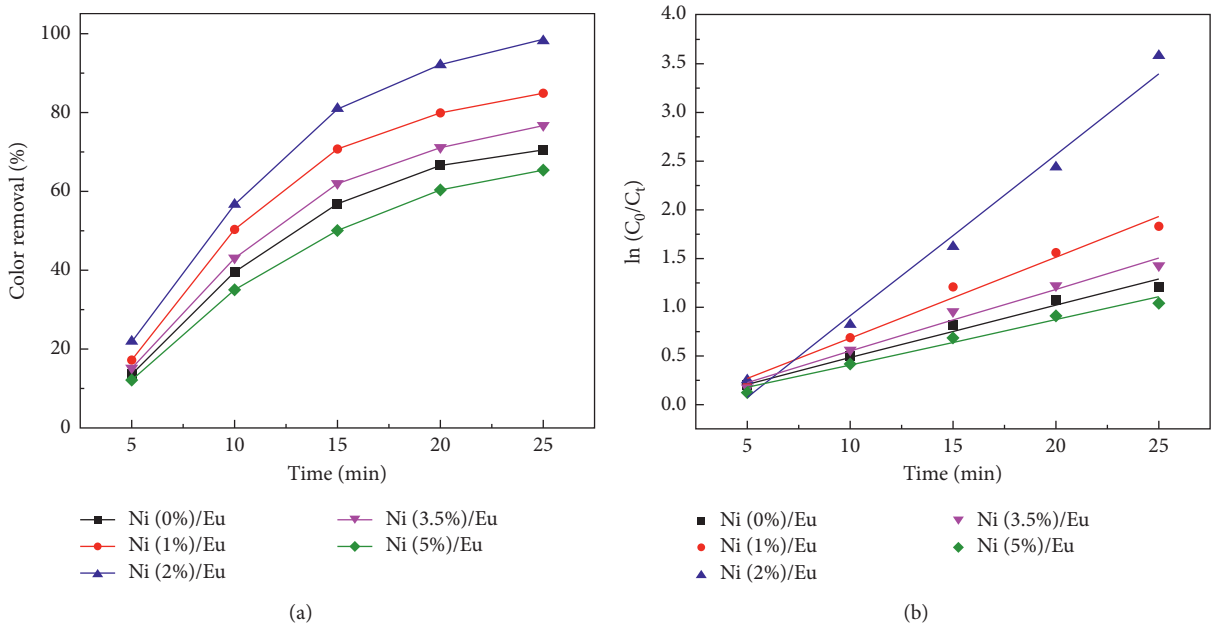

Figure 11: Electrochemical decolorization performance at Ti/SnO_2-Sb-Ni/Eu electrodes modified with various Ni contents. (a) Decolorization efficiency. (b) Kinetic analysis of the curves (RhB concentration: 20 mg·L^{-1}; current density: 10 mA·cm^{-2}; supporting electrolyte: 0.1 mol·$L^{-1}$$Na_2SO_4$; 25°C).

Table 6: Kinetic parameters of 20 mg·L^{-1} RhB in electrochemical processes by Ti/SnO_2-Sb-Ni/Eu electrodes modified with various Ni contents.

	Ni (0%)/Eu	Ni (1%)/Eu	Ni (2%)/Eu	Ni (3.5%)/Eu	Ni (5%)/Eu
Rate constants (k) (min^{-1})	0.0539	0.0634	0.1727	0.0361	0.0084
R^2	0.9716	0.9822	0.9769	0.9915	0.9922

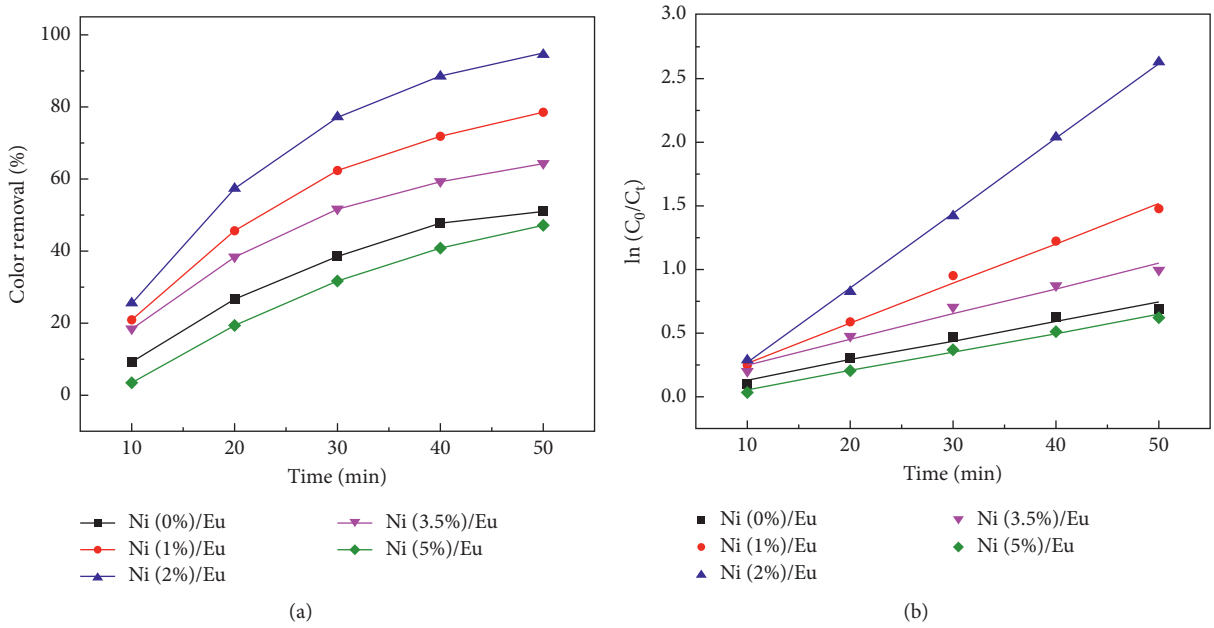

Figure 12: Electrochemical decolorization performance at Ti/SnO_2-Sb-Ni/Eu electrodes modified with various Ni contents. (a) Decolorization efficiency. (b) Kinetic analysis of the curves (RhB concentration: 40 mg·L^{-1}; current density: 10 mA·cm^{-2}; supporting electrolyte: 0.1 mol·L^{-1}Na_2SO_4; 25°C).

Table 7: Kinetic parameters of 40 mg·L^{-1} RhB in electrochemical processes by Ti/SnO_2-Sb-Ni/Eu electrodes modified with various Ni contents.

	Ni (0%)/Eu	Ni (1%)/Eu	Ni (2%)/Eu	Ni (3.5%)/Eu	Ni (5%)/Eu
Rate constants (k) (min^{-1})	0.0152	0.0312	0.0589	0.0199	0.0147
R^2	0.9718	0.9933	0.9995	0.9766	0.9916

the second segment intersects the axes (x, y) is the OEP of the electrode [24]. Comparing the OEP of Ti/SnO_2-Sb-Ni/Re electrodes exhibits that the Ni (2%)/Gd electrode shows the highest OEP of 2.083 V while those of the electrodes prepared without Ni intermediate layer were lower. The OEP of the Ni (2%)/Ce, Ni (2%)/Eu, and Ni (2%)/Er electrodes was 2.013 V, 2.038 V, and 2.021 V, respectively. When the OEP is high, fewer side reactions observe less unwanted power loss and enhancing organic pollutants degradation efficiency [39]. Accordingly, the doping Ni (2%) contents in the intermediate layer can raise the decolorization capacity of the electrodes.

3.3. Decolorization of Rhodamine B. As shown in Figure 7(a), it can be seen that the decolorization efficiencies could reach 99%, 75%, 60%, 55%, and 53% for Ni (2%), Ni (1%), Ni (3.5%), Ni (5%), and Ni (0%) doped with Gd coating layer, respectively. After 25 min electrolysis, the decolorization rate was observed at the Ni (2%) modified Gd electrode which was more than 6.6 times those at the Ni (0%) modified Gd electrodes at the initial RhB concentration of 20 mg L^{-1} (Table 2, Figure 7(b)). At the concentration of 40 mg L^{-1}, the decolorization efficiencies of Gd doped electrodes modified with Ni (2%), Ni (1%), Ni (3.5%), Ni (5%), and Ni (0%) reached 98%, 90%, 80%, 75%, and 62%, respectively (Figure 8(a)). The decolorization rates of the Ni (2%) modified Gd electrode reported in Table 3 and Figure 8(b) were 3.9 times faster than those of Ni (0%) modified Gd electrode during the experimental time for 50 min.

Figure 9(a) presents 92%, 84%, 67%, 61%, and 56% of the decolorization efficiencies for Ni (2%), Ni (1%), Ni (0%), Ni (5%), and Ni (3.5%) contents doped with Ce coating layer,

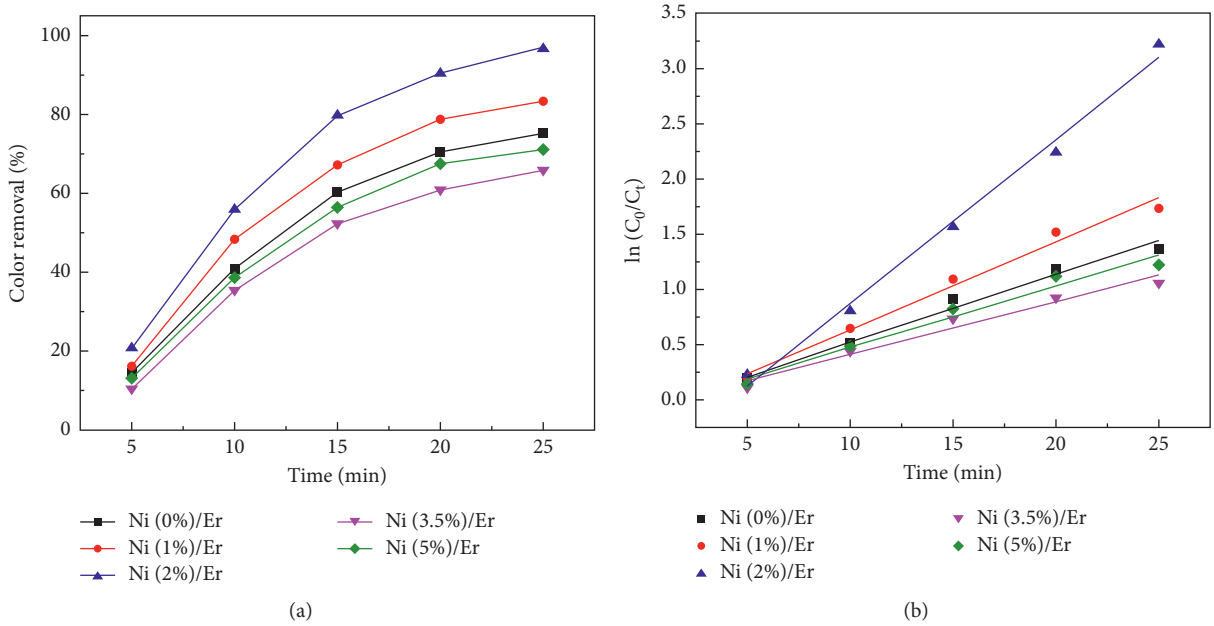

FIGURE 13: Electrochemical decolorization performance at Ti/SnO_2-Sb-Ni/Er electrodes modified with various Ni contents. (a) Decolorization efficiency. (b) Kinetic analysis of the curves (RhB concentration: 20 mg·L^{-1}; current density: 10 mA·cm^{-2}; supporting electrolyte: 0.1 mol·$L^{-1}$$Na_2SO_4$; 25°C).

TABLE 8: Kinetic parameters of 20 mg·L^{-1} RhB in electrochemical processes by Ti/SnO_2-Sb-Ni/Er electrodes modified with various Ni contents.

	Ni (0%)/Er	Ni (1%)/Er	Ni (2%)/Er	Ni (3.5%)/Er	Ni (5%)/Er
Rate constants (k) (min^{-1})	0.0618	0.0797	0.1486	0.0477	0.0557
R^2	0.9806	0.9842	0.9919	0.9709	0.9735

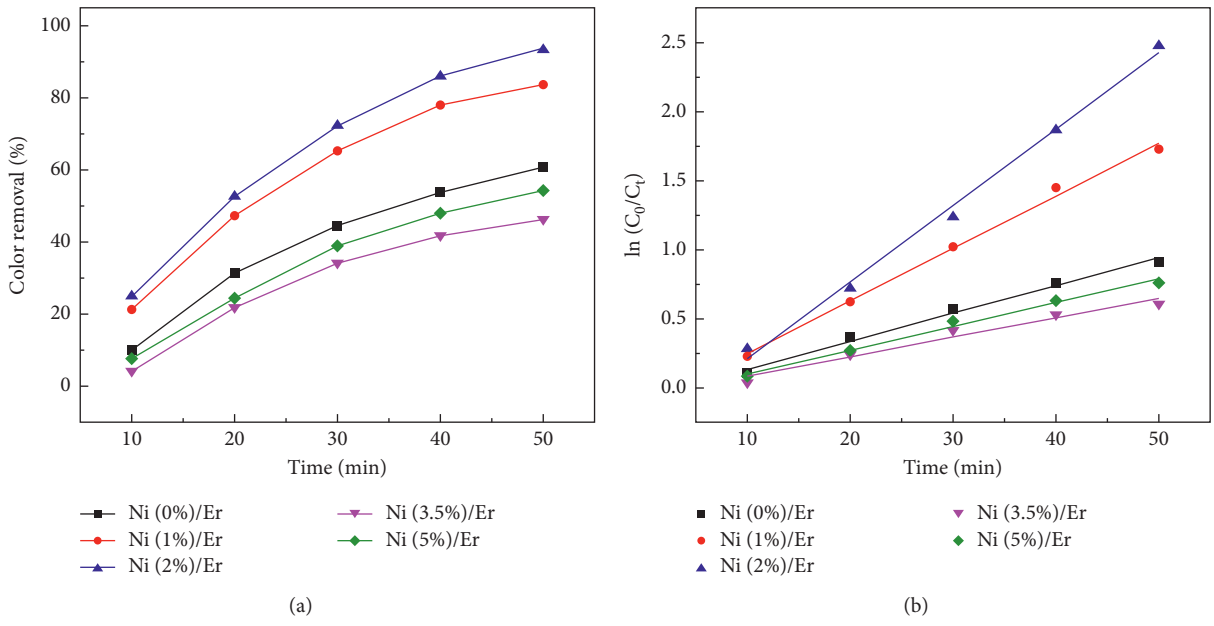

FIGURE 14: Electrochemical decolorization performance at Ti/SnO_2-Sb-Ni/Er electrodes modified with various Ni contents. (a) Decolorization efficiency. (b) Kinetic analysis of the curves (RhB concentration: 40 mg·L^{-1}; current density: 10 mA·cm^{-2}; supporting electrolyte: 0.1 mol·$L^{-1}$$Na_2SO_4$; 25°C).

Table 9: Kinetic parameters of 40 mg·L^{-1} RhB in electrochemical processes by Ti/SnO_2-Sb-Ni/Er electrodes modified with various Ni contents.

	Ni (0%)/Er	Ni (1%)/Er	Ni (2%)/Er	Ni (3.5%)/Er	Ni (5%)/Er
Rate constants (k) (min^{-1})	0.02	0.038	0.0554	0.0142	0.0173
R^2	0.989	0.9959	0.9949	0.9709	0.9904

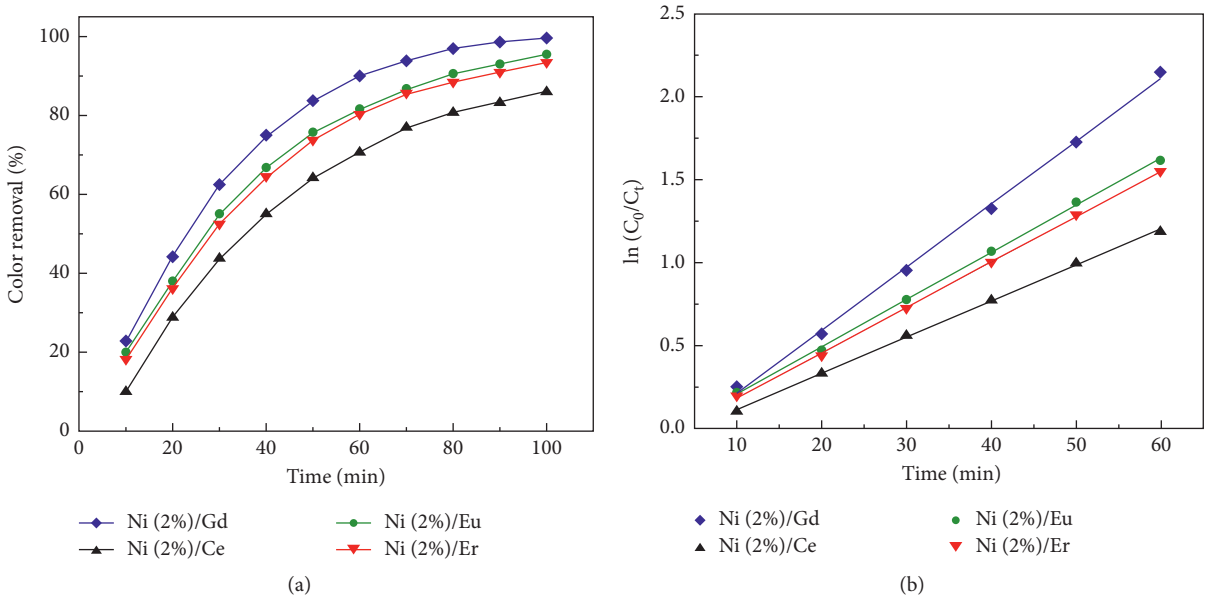

Figure 15: Electrochemical decolorization performance at Ti/SnO_2-Sb-Ni/Re (Re = Gd, Ce, Eu, Er) electrodes modified with Ni (2%) content. (a) Decolorization efficiency. (b) Kinetic analysis of the curves (RhB concentration: 100 mg·L^{-1}; current density: 10 mA·cm^{-2}; supporting electrolyte: 0.1 mol·L^{-1}Na_2SO_4; 25°C).

Table 10: Kinetic parameters of 100 mg·L^{-1} RhB in electrochemical processes by Ti/SnO_2-Sb-Ni/Re (Re = Gd, Ce, Eu, Er) electrodes modified with Ni (2%) content.

	Ni (2%)/Gd	Ni (2%)/Ce	Ni (2%)/Eu	Ni (2%)/Er
Rate constants (k) (min^{-1})	0.038	0.0218	0.0285	0.0274
R^2	0.9981	0.9991	0.9991	0.9995

respectively. After 25 min treatment, the decolorization rate of the Ni (2%) modified Ce electrode was more than 2.3 times that of the Ni (0%) modified Ce electrode using an initial concentration of 20 mg·L^{-1} (Table 4 and Figure 9(b)). It can be observed from Figure 10(a) that the decolorization efficiencies of Ce doped (40 mg·L^{-1}) initial concentration (50 min treatment time) which was modified with Ni (2%), Ni (1%), Ni (0%), Ni (3.5%), and Ni (5%) were reduced to 90%, 71%, 47%, 43%, and 41% respectively. Table 5 and Figure 10(b) show that the decolorization rate on the Ni (2%) modified Ce electrode performed was 3.6 times faster than that on the Ni (0%) modified Ce electrode.

Figure 11(a) shows that 98%, 85%, 77%, 71%, and 65% of the decolorization efficiencies were achieved for Ni (2%), Ni (1%), Ni (3.5%), Ni (0%), and Ni (5%) doped with Eu electrodes, respectively. The decolorization rate of the Ni-(2%) modified Eu electrode was found 3.2 times faster than that of the Ni- (0%) modified Eu electrode using an initial concentration of 20 mg·L^{-1} after 25 min presented in Figure 11(b) and Table 6. The experimental condition was changed only at the initial concentration of 40 mg·L^{-1}, and the decolorization efficiencies of Eu doped electrodes which were modified with Ni (2%), Ni (1%), Ni (3.5%), Ni (0%), and Ni (5%) were decreased to 95%, 79%, 64%, 51%, and 47%, respectively (Figure 12(a)). Table 7 displays that the decolorization rate of the Ni (2%) modified Eu electrode was 3.8 times faster than that of the Ni (0%) modified Eu electrode after 50 min experimental time (Figure 12(b)).

According to Figure 13(a), the decolorization efficiencies could reach 97%, 83%, 75%, 71%, and 65% for 2 at. %, 1 at. %, 0 at. %, 5 at. %, and 3.5 at. % Ni contents, respectively. After 25 min electrolysis by using 20 mg·L^{-1} RhB, the

Table 11: Energy per order of decolorized 20 mg·L^{-1} RhB solution, evaluated from equation (5), and electrochemical decolorization of Ti/SnO_2-Sb-Ni/Re electrodes with various Ni contents and different rare earth elements in 200 ml dye solution.

Electrodes	k_{app} (min^{-1})	Average voltage (V)	Energy (kW·h·m^{-3}·order^{-1}
Ni (0%)/Gd	0.0316	4.2	4.253
Ni (1%)/Gd	0.0554	4.2	2.426
Ni (2%)/Gd	0.2094	4.1	0.627
Ni (3.5%)/Gd	0.0366	4.1	3.585
Ni (5%)/Gd	0.0322	4	3.975
Ni (0%)/Ce	0.0476	4.1	2.756
Ni (1%)/Ce	0.0817	4.2	1.645
Ni (2%)/Ce	0.109	4.1	1.204
Ni (3.5%)/Ce	0.0409	4	3.129
Ni (5%)/Ce	0.0364	4	3.516
Ni (0%)/Eu	0.0539	4.2	2.494
Ni (1%)/Eu	0.0634	4.2	2.119
Ni (2%)/Eu	0.1727	4.1	0.759
Ni (3.5%)/Eu	0.0361	4.2	3.723
Ni (5%)/Eu	0.0084	4	15.238
Ni (0%)/Er	0.0618	4.2	2.175
Ni (1%)/Er	0.0797	4.1	1.646
Ni (2%)/Er	0.1486	4.2	0.904
Ni (3.5%)/Er	0.0477	4	2.683
Ni (5%)/Er	0.0557	4	2.298

Current intensity = 10 mA·cm^{-2}, electrolyte = 0.1 mol·L^{-1} Na_2SO_4, and temperature = 25°C.

Table 12: Energy per order of decolorized 40 mg·L^{-1} RhB solution, evaluated from equation (5), and electrochemical decolorization of Ti/SnO_2-Sb-Ni/Re electrodes with various Ni contents and different rare earth elements in 200 ml dye solution.

Electrodes	k_{app} (min^{-1})	Average voltage (V)	Energy (kW·h·m^{-3}·order^{-1})
Ni (0%)/Gd	0.0221	4.5	6.516
Ni (1%)/Gd	0.045	4.4	3.129
Ni (2%)/Gd	0.0861	4.1	1.524
Ni (3.5%)/Gd	0.0335	4.1	3.916
Ni (5%)/Gd	0.0306	4	4.183
Ni (0%)/Ce	0.0136	4.3	10.11
Ni (1%)/Ce	0.0265	4.2	5.071
Ni (2%)/Ce	0.0498	4.1	2.634
Ni (3.5%)/Ce	0.0121	4	10.578
Ni (5%)/Ce	0.0116	4.1	11.310
Ni (0%)/Eu	0.0152	4.5	9.474
Ni (1%)/Eu	0.0312	4.4	4.513
Ni (2%)/Eu	0.0589	4.3	2.336
Ni (3.5%)/Eu	0.0199	4.1	6.593
Ni (5%)/Eu	0.0147	4.2	9.143
Ni (0%)/Er	0.02	4.6	7.361
Ni (1%)/Er	0.038	4.1	3.453
Ni (2%)/Er	0.0554	4.1	2.368
Ni (3.5%)/Er	0.0142	4	9.014
Ni (5%)/Er	0.0173	4.1	7.584

Current intensity = 10 mA·cm^{-2}, electrolyte = 0.1 mol·L^{-1} Na_2SO_4, and temperature = 25°C.

decolorization rate observed at the Ni (2%) modified Ce electrode was 2.4 times faster than Ni (0%) modified Er electrode (Table 8 and Figure 13(b)). Figure 14(a) represents that the decolorization efficiencies of Er-doped electrodes using 40 mg·L^{-1} RhB which was modified with 2 at. %, 1 at. %, 0 at. %, 5 at. %, and 3.5 at. % Ni contents reached 93%, 84%, 61%, 54%, and 46%, respectively. Figure 14(b) displays the decolorization rate of the Ni (2%) modified Er electrode which was 2.8 times faster than that of the Ni (0%) modified Er electrode after 50 min degradation time (Table 9).

According to the decolorization results of 20 mg·L^{-1} and 40 mg·L^{-1} dye concentration, there was a very good performance of the Ni (2%) modified rare earth electrodes, and therefore, these electrodes were further examined to evaluate the electrochemical degradation of 100 mg·L^{-1} RhB (Figures 15(a) and 15(b)). The Ni (2%) modified Gd electrode

Table 13: Energy per order of decolorized 100 mg·L^{-1} RhB solution, evaluated from equation (5), and electrochemical decolorization of Ti/SnO_2-Sb-Ni/Re electrodes with Ni (2%) content and different rare earth elements in 200 ml dye solution.

Electrodes	k_{app} (min^{-1})	Average voltage (V)	Energy (kW·h·m^{-3}·order^{-1})
Ni (2%)/Gd	0.038	4.3	3.621
Ni (2%)/Ce	0.0218	4.3	6.312
Ni (2%)/Eu	0.0285	4.4	4.940
Ni (2%)/Er	0.0274	4.4	5.138

Current intensity = 10 mA cm^{-2}, electrolyte = 0.1 mol. L^{-1} Na_2SO_4, and temperature = 25°C.

presented the best performance and reached the highest decolorized of 90% after 60 min electrolysis treatment. This was 8.3% higher than Ni (2%) modified Eu electrode, 20% higher than Ni (2%) modified Ce electrode, and 9.8% higher than Ni (2%) modified Er electrode. These removal efficiencies of the as-prepared electrodes were better than those of the PbO_2/Sb-SnO_2/TiO_2 NTAs electrode [40] which removed 40% of color after 60 min at the experimental condition (20 mA·cm^{-2} current density, 100 mg·L^{-1} RhB, and 0.1 mol·L^{-1} Na_2SO_4). Table 10 presents the kinetic rate constant of the Gd electrode with Ni (2%) content electrode which was 2.2 times, 1.7 times, and 1.8 times faster than that of Ce, Eu, and Er with Ni (2%) content electrodes.

All of the abovementioned results reported that the modified Ni intermediate layer-based rare earth electrodes significantly improve the performance of electrochemical decolorization of RhB. In the cases of organic substances oxidation, hydroxyl radicals ($^{\cdot}$OH) which were initiated from H_2O oxidation (equation (2)) act as a mediator. The $^{\cdot}$OH can either accelerate the oxidation of the organic pollutants (equation (3)).

$$M + H_2O \longrightarrow M(^{\cdot}OH)_n + nH^+ + ne^- \quad (2)$$

$$R + M(^{\cdot}OH)_n \longrightarrow M + \text{Oxidation products}(\text{such as } CO_2) + nH^+ + ne^- \quad (3)$$

In other reports, the color removing kinetics effort on each electrode was observed to be related properly to the pseudo-first-order [40–42]. The dye concentration decreased exponentially with time and the kinetic rate can be assessed by the following mathematical formula [43]:

$$\ln\left(\frac{C_0}{C_t}\right) = k_{app}t, \quad (4)$$

where C_0 and C_t are the dye concentration (mg·L^{-1}) at the initial condition and at experimental time t, respectively. The k_{app} (min^{-1}) is the detected rate constant.

The reduction in energy demands is one of the curial potions in ascertaining the achievability of the electrocatalytic destruction of organic contaminants. The magnitude of electrical energy (kWh) needed to decrease the concentration of contaminant in a unit volume (1000 dm^3) by one order of magnitude was defined as electric energy per order (E_{EO}) due to the decolorization kinetics of RhB obeyed pseudo-first-order. The values of E_{EO} (kW h m^{-3} order^{-1}) can be evaluated from the following equation [43]:

$$E_{EO} = \frac{38.4 \times P}{k_1' \times V}, \quad (5)$$

where P is the electrical power (kW), V is the volume of dye solution (m^3), and k_1' is the pseudo-first-order rate constant.

Table 11 presents the variation of the energy per order for the electrochemical decolorization on Ti/SnO_2-Sb-Ni/Re electrodes for various Ni contents and different rare earth elements at a dye concentration of 20 mg·L^{-1}. According to these results, the value of E_{EO} is 6.8 times lower for the Ni (2%)/Gd electrode than for the Ni (0%)/Gd electrode, reduced to 2.3 times lower for the Ni (2%)/Ce than for the Ni (0%)/Ce, decreased 3.3 times lower for the Ni (2%)/Eu than for the Ni (0%)/Eu, and down to 2.4 times lower for the Ni (2%)/Er than for the Ni (0%)/Er. The resultant values of E_{EO} were observed in Table 12 which is the decolorization of 40 mg·L^{-1} initial concentration. It can be observed that the value of E_{EO} decreased at the Ni (2%)/Gd electrode. This value is 4.3 times lower than that of the Ni (0%)/Gd electrode applied. The value of E_{EO} for the Ni (2%)/Ce electrode is 3.8 times lower than that of the Ni (0%)/Ce electrode, reduced to 4 times lower for the Ni (2%)/Eu than for the Ni (0%)/Eu, and declined 3.1 times lower for the Ni (2%)/Er than for the Ni (0%)/Er. Table 13 shows the variation of the energy per order on Ti/SnO_2-Sb-Ni/Re electrodes with Ni (2%) at 100 mg L^{-1} dye concentration. The value of E_{EO} for the Gd electrode is 1.7 times, 1.3 times, and 1.4 times lower than that of the Ce, Eu, and Er electrodes, respectively. The E_{EO} values presented here demonstrate that the use of Ni (2%) intermediate layer was energy savings against other Ni content modified electrodes.

3.4. Electrode Stability Tests. Electrode strength is a prominent aspect that concludes whether Ti- and Sn-based electrodes are to be exploited in the industrial range. The service life is acutely dominated by the experimental circumstances: temperature, current density, and electrolyte concentration. The real service lifetime of electrodes, because of utilization at moderate current density operation, is comparatively lengthy, which is inconvenient to be evaluated. Since Correa-Lozano et al. have introduced the experimental correlation between the actual lifetime (t_1) and the accelerated lifetime (t_2), this correlation was employed to estimate the actual service time of Ti- and Sn-based anodes at various current densities [44], as displayed in

$$t_1 = \left(\frac{i_2}{i_1}\right)^2 t_2, \quad (6)$$

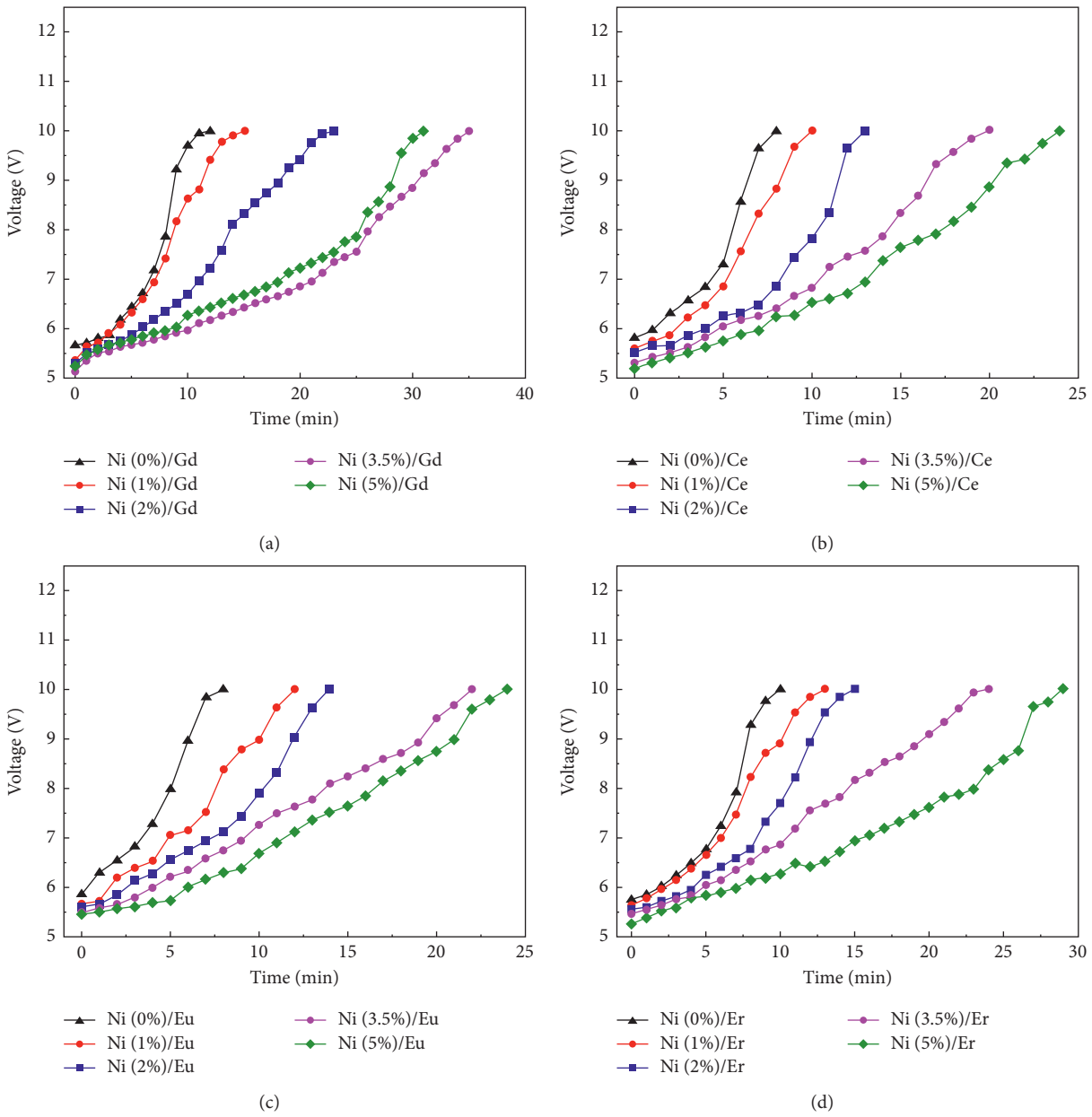

FIGURE 16: Accelerated life curves of Ti/SnO_2-Sb-Ni/Re electrodes modified with various Ni contents in 1.0 mol·L^{-1} H_2SO_4 with a current density of 1000 mA·cm^{-2} at 40°C (Re = (a) Gd, (b) Ce, (c) Eu, and (d) Er electrodes).

where i_1 is the current density (10 mA·cm^{-2}) for the actual condition. And i_2 is the current density for the accelerated test [26].

In this work, the test conditions for accelerated duration are comparatively high, with a current density (1000 mA·cm^{-2}), concentrated sulfuric acid solution (1.0 mol·L^{-1}), and temperature (40°C). Thus, the electrode accelerated service time acquired during this condition is comparatively short. Figures 16(a)–16(d) exhibit the accelerated service life of Ti/SnO_2-Sb-Ni/Re electrodes modified with various Ni contents. Table 14 displays the accelerated lifetime of Ti-based Sb-SnO_2 electrodes studied by other researchers and the experimental results of this study. These obtained data are transformed into actual service duration by equation (6). The increased actual life was observed in the electrode content with Ni (3.5% and 5%) compared with other electrodes. The rare earth Gd, Ce, Eu, and Er with intermediate layer Ni (2%) electrodes show that the service life is higher than those electrodes without the Ni layer. This can summarize that the service life of Ti/SnO_2-Sb-Re electrodes can be improved by incorporating different content Ni intermediate layers. This progress may appear when the intermediate layer potently prohibits the damage of the electrolyte or other active materials penetrate the active layer to meet the Ti medium. This condition will lead to the formation of an insulating layer of TiO_2 at the site of the electrode surface and can deactivate the electrode. Simultaneously, the evolved oxygen damaging the coated film

Table 14: Accelerated lifetime and practical lifetime data for Ti/SnO_2-Sb electrodes in some previous works and this work.

Electrode types	Operated condition	Current density ($mA \cdot cm^{-2}$)	Accelerated lifetime (h)	Experimental lifetime (h) Current density 10 ($mA \cdot cm^{-2}$)	Ref.
Ti/SnO_2-Sb/Gd			0.2	2000	
Ti/SnO_2-Sb-Ni (1%)/Gd			0.25	2500	
Ti/SnO_2-Sb-Ni (2%)/Gd			0.38	3800	
Ti/SnO_2-Sb-Ni (3.5%)/Gd			0.58	5800	
Ti/SnO_2-Sb-Ni (5%)/Gd			0.51	5100	
Ti/SnO_2-Sb/Ce			0.13	1300	
Ti/SnO_2-Sb-Ni (1%)/Ce			0.16	1600	
Ti/SnO_2-Sb-Ni (2%)/Ce			0.22	2200	
Ti/SnO_2-Sb-Ni (3.5%)/Ce			0.33	3300	
Ti/SnO_2-Sb-Ni (5%)/Ce	1M H_2SO_4, 40°C	1000	0.4	4000	This study
Ti/SnO_2-Sb/Eu			0.13	1300	
Ti/SnO_2-Sb-Ni (1%)/Eu			0.2	2000	
Ti/SnO_2-Sb-Ni (2%)/Eu			0.23	2300	
Ti/SnO_2-Sb-Ni (3.5%)/Eu			0.36	3600	
Ti/SnO_2-Sb-Ni (5%)/Eu			0.4	4000	
Ti/SnO_2-Sb/Er			0.17	1700	
Ti/SnO_2-Sb-Ni (1%)/Er			0.21	2100	
Ti/SnO_2-Sb-Ni (2%)/Er			0.25	2500	
Ti/SnO_2-Sb-Ni (3.5%)/Er			0.4	4000	
Ti/SnO_2-Sb-Ni (5%)/Er			0.48	4800	
Ti/Cu-NRs/Sb-SnO_2	0.5 M H_2SO_4	1000	0.2	2000	[26]
Ti/TiO_2/SbO_2-SnO_2 /SnO_2-Sb-CeO_2	1M H_2SO_4	300	1.84	1656	[45]
Ti/Mn-Sb-SnO_2	0.25 M Na_2SO_4	100	35	3500	[46]
Ti/SnO_2-Sb	0.25 M Na_2SO_4	100	6	600	[47]
Ti/Sb-SnO_2-GNS			18.1	1810	
Ti/Sb-SnO_2-NGNS			26.7	2670	
Ti/Sb-SnO_2-Ce	0.25 M Na_2SO_4	100	8.7	870	[48]

of the electrode prohibits the outer layer from fall down, in that way extending the lifetime of the electrode and the passivation will be delayed [49–51].

4. Conclusions

The Ti/SnO_2-Sb-Ni/Re electrodes obtained are very helpful for the electrochemical degradation of RhB. Compared with Ti/SnO_2-Sb-Ni/Re, experimental results exhibited that these modified electrodes had a different electrochemical decolorization performance. Compared with modified Ni (0%, 1%, and 2%)/Re electrodes, the longer accelerated life could be observed in Ni (3.5%)/Re and Ni (5%)/ Re electrodes. Compared to those without intermediate layer electrodes, the electrodes with Ni (2%) intermediate layers exhibited increased electrochemical performance and efficiency for decolorization of RhB. Additionally, their service lifetimes increased more than 1.9 times, 1.69 times, 1.76 times, and 1.47 times for Gd, Ce, Eu, and Er, respectively. Compared with the color removal efficiencies of the Ni (2%)/Re electrodes of decolorization efficiencies, the color removal rate of RhB reaches 90% after treatment for 60 min. Relatively low energy consumption of 3.621 kWh m^{-3} of wastewater can be acquired under the experimental condition of 100 $mg \cdot L^{-1}$ RhB. It is concluded that the moderate content Ni could enhance the decolorization performance, but higher Ni amounts did not result in better performance.

Data Availability

The data used to support the findings of this study are included within the article.

Conflicts of Interest

The authors declare that there are no conflicts of interest regarding the publication of this paper.

Acknowledgments

This work was supported by Zenghe Li as a funder, corresponding author at Beijing Key Laboratory of Environmentally Harmful Chemical Analysis, College of Chemistry, Beijing University of Chemical Technology, Beijing 100029, China.

References

[1] M. Abbasi, A. R. Soleymani, and J. B. Parsa, "Degradation of Rhodamine B by an electrochemical ozone generating system consist of a Ti anode coated with nanocomposite of Sn-Sb-Ni oxide," *Process Safety and Environmental Protection*, vol. 94, pp. 140–148, 2015.

[2] L. Du, J. Wu, and C. Hu, "Electrochemical oxidation of Rhodamine B on RuO_2-PdO-TiO_2/Ti electrode," *Electrochimica Acta*, vol. 68, pp. 69–73, 2012.

[3] M. Kornaros and G. Lyberatos, "Biological treatment of wastewaters from a dye manufacturing company using a

trickling filter," *Journal of Hazardous Materials*, vol. 136, no. 1, pp. 95–102, 2006.

[4] H. Ouachtak, R. El Haouti, A. El Guerdaoui et al., "Experimental and molecular dynamics simulation study on the adsorption of Rhodamine B dye on magnetic montmorillonite composite γ-Fe_2O_3@Mt," *Journal of Molecular Liquids*, vol. 309, Article ID 113142, 2020.

[5] M. Khayet, A. Y. Zahrim, and N. Hilal, "Modelling and optimization of coagulation of highly concentrated industrial grade leather dye by response surface methodology," *Chemical Engineering Journal*, vol. 167, no. 1, pp. 77–83, 2011.

[6] W. X. Jiang, W. Zhang, and B. J. Li, "Combined fenton oxidation and biological activated carbon process for recycling of coking plant effluent," *Journal of Hazardous Materials*, vol. 189, no. 1-2, pp. 308–314, 2011.

[7] A. Y. Zahrim and N. Hilal, "Treatment of highly concentrated dye solution by coagulation/flocculation-sand filtration and nanofiltration," *Water Resources and Industry*, vol. 3, pp. 23–34, 2013.

[8] F. Alakhras, E. Alhajri, R. Haounati, H. Ouachtak, A. A. Addi, and T. A. Saleh, "A comparative study of photocatalytic degradation of Rhodamine B using natural-based zeolite composites," *Surfaces and Interfaces*, vol. 20, p. 100611, 2020.

[9] X.-b. Zhang, W.-y. Dong, and W. Yang, "Decolorization efficiency and kinetics of typical reactive azo dye RR2 in the homogeneous Fe(II) catalyzed ozonation process," *Chemical Engineering Journal*, vol. 233, pp. 14–23, 2013.

[10] M. Abbasi and N. Asl, "Sonochemical degradation of Basic Blue 41 dye assisted by nanoTiO_2 and H_2O_2," *Journal of Hazardous Materials*, vol. 153, no. 3, pp. 942–947, 2008.

[11] C. A. Martinez-Huitle and E. Brillas, "Decontamination of wastewaters containing synthetic organic dyes by electrochemical methods: a general review," *Applied Catalysis B-Environmental*, vol. 87, no. 3-4, pp. 105–145, 2009.

[12] M. Faouzi, P. Cañizares, A. Gadri et al., "Advanced oxidation processes for the treatment of wastes polluted with azoic dyes," *Electrochimica Acta*, vol. 52, no. 1, pp. 325–331, 2006.

[13] N. Bensalah, A. Bedoui, S. Chellam, and A. Abdel-Wahab, "Electro-Fenton treatment of photographic processing wastewater," *CLEAN—Soil, Air, Water*, vol. 41, no. 7, pp. 635–644, 2013.

[14] T. Coşkun, E. Debik, and N. M. Demır, "Operational cost comparison of several pre-treatment techniques for OMW treatment," *CLEAN—Soil, Air, Water*, vol. 40, no. 1, pp. 95–99, 2012.

[15] C. Indermuhle, M. J. Martín de Vidales, C. Sáez et al., "Degradation of caffeine by conductive diamond electrochemical oxidation," *Chemosphere*, vol. 93, no. 9, pp. 1720–1725, 2013.

[16] H. Wang and Y. M. Huang, "Prussian-blue-modified iron oxide magnetic nanoparticles as effective peroxidase-like catalysts to degrade methylene blue with H_2O_2," *Journal of Hazardous Materials*, vol. 191, no. 1-3, pp. 163–169, 2011.

[17] C. A. Martínez-Huitle and S. Ferro, "Electrochemical oxidation of organic pollutants for the wastewater treatment: direct and indirect processes," *Chemical Society Reviews*, vol. 35, no. 12, pp. 1324–1340, 2006.

[18] E. Guinea, E. Brillas, F. Centellas, P. Cañizares, M. A. Rodrigo, and C. Sáez, "Oxidation of enrofloxacin with conductive-diamond electrochemical oxidation, ozonation and Fenton oxidation. A comparison," *Water Research*, vol. 43, no. 8, pp. 2131–2138, 2009.

[19] A. Novoselova and V. Smolenski, "Electrochemical behavior of neodymium compounds in molten chlorides," *Electrochimica Acta*, vol. 87, pp. 657–662, 2013.

[20] Y. Duan, Y. Chen, Q. Wen, and T. Duan, "Fabrication of dense spherical and rhombic Ti/Sb-SnO_2 electrodes with enhanced electrochemical activity by colloidal electrodeposition," *Journal of Electroanalytical Chemistry*, vol. 768, pp. 81–88, 2016.

[21] T. Duan, Y. Chen, Q. Wen, and Y. Duan, "Different mechanisms and electrocatalytic activities of Ce ion or CeO_2 modified Ti/Sb-SnO_2 electrodes fabricated by one-step pulse electro-codeposition," *RSC Advances*, vol. 5, no. 25, pp. 19601–19612, 2015.

[22] Y. Wang, C. Shen, M. Zhang, B.-T. Zhang, and Y.-G. Yu, "The electrochemical degradation of ciprofloxacin using a SnO_2-Sb/Ti anode: influencing factors, reaction pathways and energy demand," *Chemical Engineering Journal*, vol. 296, pp. 79–89, 2016.

[23] Z. Zhang, Q. Q. Sun, and Y. P. Si, "Degradation properties of Ti/Sb-SnO2 electrodes containing different intermediate layers for phenol," in *Materials Science Forum*Trans Tech Publications, Zurich, Switzerland, 2013.

[24] Q. Bi, W. Guan, Y. Gao, Y. Cui, S. Ma, and J. Xue, "Study of the mechanisms underlying the effects of composite intermediate layers on the performance of Ti/SnO_2-Sb-La electrodes," *Electrochimica Acta*, vol. 306, pp. 667–679, 2019.

[25] D. Shao, W. Yan, X. Li, H. Yang, and H. Xu, "A highly stable Ti/TiHx/Sb-SnO_2 anode: preparation, characterization and application," *Industrial & Engineering Chemistry Research*, vol. 53, no. 10, pp. 3898–3907, 2014.

[26] L. Xu, M. Li, and W. Xu, "Preparation and characterization of Ti/SnO2-Sb electrode with copper nanorods for AR 73 removal," *Electrochimica Acta*, vol. 166, pp. 64–72, 2015.

[27] X. Li, D. Shao, H. Xu, W. Lv, and W. Yan, "Fabrication of a stable Ti/TiO x H y/Sb–SnO_2 anode for aniline degradation in different electrolytes," *Chemical Engineering Journal*, vol. 285, pp. 1–10, 2016.

[28] J. Z. Hu, P. C. Deng, and X. W. Wang, "Stable Ti/IrO_2 anode with iridium-titanium oxide interlayers for O_2 evolution," in *Materials Science Forum*Trans Tech Publications, Zurich, Switzerland, 2011.

[29] C. Shao, J. Yu, X. Li, X. Wang, and K. Zhu, "Influence of the Pt nanoscale interlayer on stability and electrical property of Ti/Pt/Sb-SnO_2 electrode: a synergetic experimental and computational study," *Journal of Electroanalytical Chemistry*, vol. 804, pp. 140–147, 2017.

[30] G. Zhao, X. Cui, M. Liu et al., "Electrochemical degradation of refractory pollutant using a novel microstructured TiO_2 nanotubes/Sb-doped SnO_2 electrode," *Environmental Science & Technology*, vol. 43, no. 5, pp. 1480–1486, 2009.

[31] C. F. C. Machado, M. A. Gomes, and R. S. Silva, "Time and calcination temperature influence on the electrocatalytic efficiency of Ti/SnO_2: Sb(5%), Gd(2%) electrodes towards the electrochemical oxidation of naphthalene," *Journal of Electroanalytical Chemistry*, vol. 816, pp. 232–241, 2018.

[32] Y. Feng, Y. Cui, B. Logan, and Z. Liu, "Performance of Gd-doped Ti-based Sb-SnO_2 anodes for electrochemical destruction of phenol," *Chemosphere*, vol. 70, no. 9, pp. 1629–1636, 2008.

[33] Y.-H. Cui, Y.-J. Feng, and Z.-Q. Liu, "Influence of rare earths doping on the structure and electro-catalytic performance of Ti/Sb-SnO_2 electrodes," *Electrochimica Acta*, vol. 54, no. 21, pp. 4903–4909, 2009.

[34] S. P. Li, X. Y. Zeng, and Y. Y. Jiang, "The study on the effect of Er on the structure and properties of Ti/SnO_2-Sb anode prepared by pechini's method," in *Advanced Materials Research*Trans Tech Publications, Zurich, Switzerland, 2013.

[35] C. A. Martínez-Huitle and M. Panizza, "Electrochemical oxidation of organic pollutants for wastewater treatment," *Current Opinion in Electrochemistry*, vol. 11, pp. 62–71, 2018.

[36] G. Chen, "Electrochemical technologies in wastewater treatment," *Separation and Purification Technology*, vol. 38, no. 1, pp. 11–41, 2004.

[37] J.-t. Kong, S.-y. Shi, X.-p. Zhu, and J.-r. Ni, "Effect of Sb dopant amount on the structure and electrocatalytic capability of Ti/Sb-SnO_2 electrodes in the oxidation of 4-chlorophenol," *Journal of Environmental Sciences*, vol. 19, no. 11, pp. 1380–1386, 2007.

[38] F. Montilla, E. Morallón, A. De Battisti, A. Benedetti, H. Yamashita, and J. L. Vázquez, "Preparation and characterization of antimony-doped tin dioxide electrodes. Part 2. XRD and EXAFS characterization," *The Journal of Physical Chemistry B*, vol. 108, no. 16, pp. 5044–5050, 2004.

[39] F. H. Oliveira, M. E. Osugi, F. M. M. Paschoal, D. Profeti, P. Olivi, and M. V. B. Zanoni, "Electrochemical oxidation of an acid dye by active chlorine generated using Ti/Sn(1−x)Ir x O_2 electrodes," *Journal of Applied Electrochemistry*, vol. 37, no. 5, pp. 583–592, 2007.

[40] J. Wu, K. Zhu, H. Xu, and W. Yan, "Electrochemical oxidation of rhodamine B by PbO_2/Sb-SnO_2/TiO_2 nanotube arrays electrode," *Chinese Journal of Catalysis*, vol. 40, no. 6, pp. 917–927, 2019.

[41] X. Ma and M. Zhou, "A comparative study of azo dye decolorization by electro-Fenton in two common electrolytes," *Journal of Chemical Technology & Biotechnology*, vol. 84, no. 10, pp. 1544–1549, 2009.

[42] D. Rajkumar and J. Kim, "Oxidation of various reactive dyes with in situ electro-generated active chlorine for textile dyeing industry wastewater treatment," *Journal of Hazardous Materials*, vol. 136, no. 2, pp. 203–212, 2006.

[43] A. Baddouh, G. G. Bessegato, M. M. Rguiti et al., "Electrochemical decolorization of Rhodamine B dye: influence of anode material, chloride concentration and current density," *Journal of Environmental Chemical Engineering*, vol. 6, no. 2, pp. 2041–2047, 2018.

[44] L. Zhang, L. Xu, J. He, and J. Zhang, "Preparation of Ti/SnO_2-Sb electrodes modified by carbon nanotube for anodic oxidation of dye wastewater and combination with nanofiltration," *Electrochimica Acta*, vol. 117, pp. 192–201, 2014.

[45] L. Zhu and Y. Wang, "Yumin, Fabrication of long-life Ti/TiO_2/SbO_2-SnO_2/SnO_2-Sb-CeO_2 electrodes and application in electrochemical wastewater treatment," *Environmental Chemistry*, vol. 33, pp. 992–998, 2014.

[46] C. Shao, A. Chen, B. Yan, Q. Shao, and K. Zhu, "Improvement of electrochemical performance of tin dioxide electrodes through manganese and antimony co-doping," *Journal of Electroanalytical Chemistry*, vol. 778, pp. 7–11, 2016.

[47] T. Duan, Q. Wen, Y. Chen, Y. Zhou, and Y. Duan, "Enhancing electrocatalytic performance of Sb-doped SnO_2 electrode by compositing nitrogen-doped graphene nanosheets," *Journal of Hazardous Materials*, vol. 280, pp. 304–314, 2014.

[48] K. Yang, Y. Liu, and J. Qiao, "Electrodeposition preparation of Ce-doped Ti/SnO_2-Sb electrodes by using selected addition agents for efficient electrocatalytic oxidation of methylene blue in water," *Separation and Purification Technology*, vol. 189, pp. 459–466, 2017.

[49] C. Carlesi Jara, G. R. Salazar-Banda, R. S. Arratia, J. S. Campino, and M. I. Aguilera, "Improving the stability of Sb doped Sn oxides electrode thermally synthesized by using an acid ionic liquid as solvent," *Chemical Engineering Journal*, vol. 171, no. 3, pp. 1253–1262, 2011.

[50] L. K. Xu and J. D. Scantlebury, "A study on the deactivation of an IrO_2-Ta_2O_5 coated titanium anode," *Corrosion Science*, vol. 45, no. 12, pp. 2729–2740, 2003.

[51] F. Vicent, E. Morallon, C. Quijada, J. Vazquez, A. Aldaz, and F. Cases, "Characterization and stability of doped SnO_2 anodes," *Journal of Applied Electrochemistry*, vol. 28, no. 6, pp. 607–612, 1998.